

# Microporous Titania Crystals with Penta-oxygen Coordination

Sicong Ma, Si-Da Huang, Ya-Hui Fang, and Zhi-Pan Liu\*<sup>✉</sup>

Collaborative Innovation Center of Chemistry for Energy Material, Shanghai Key Laboratory of Molecular Catalysis and Innovative Materials, Key Laboratory of Computational Physical Science, Department of Chemistry, Fudan University, Shanghai 200433, China

**S** Supporting Information

**ABSTRACT:** Porous materials play an important role in various chemistry applications. Here with a large amount of data from global potential energy surface calculations of titania  $\text{TiO}_2$ , we identify a class of new microporous  $\text{TiO}_2$  crystals,  $\text{TiO}_2(\text{TB})$ , featuring the largest known pore size (5.6–6.7 Å) for  $\text{TiO}_2$  crystals and an unprecedented  $[\text{TiO}_5]$  trigonal bipyramid building block. Their pores are constituted by six- and eight- $[\text{TiO}_5]$  rings with the six-member ring being the most stable. While  $[\text{TiO}_5]$  coordination is traditionally regarded as an unstable unit for titania, the porous  $\text{TiO}_2(\text{TB})$  are in fact energetically more stable than the common  $\text{TiO}_2$  rutile phase and are also found to be kinetically stable at high temperatures as evident from ab initio molecular dynamics simulation. The strong ionic bonding in the Ti–O lattice is the key to stabilizing these porous materials to compensate for the weak covalent bonding in the  $[\text{TiO}_5]$  building block. By evaluating the Li-insertion energetics and structural parameters, we predict that these microporous  $\text{TiO}_2$  crystals are good candidates for Li-ion anode material.



**KEYWORDS:** microporous titania, penta-oxygen coordination, Li-ions battery, neural network potential, global potential energy surface

Titania is an important functional material with many known stable crystalline phases, ranging from common bulky phases (anatase, rutile, and so on; see Figure 1) to the

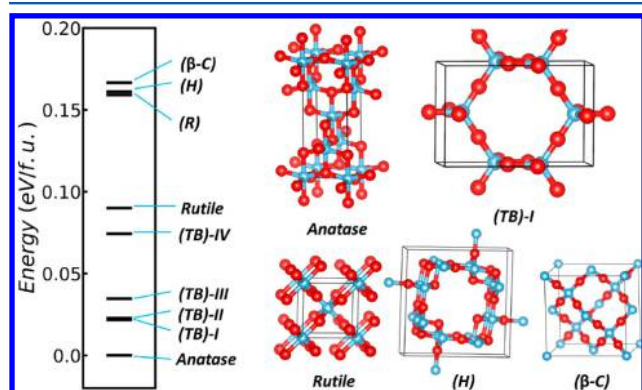


**Figure 1.** Energy spectrum for  $\text{TiO}_2$  crystals from DFT (anatase is set as the energy reference) together with the crystal structures for key  $\text{TiO}_2$  phases (also see Supporting Information for all structures): Ti, light blue balls; O, red balls.

layered phase (lepidocrocite  $\text{TiO}_2$ ).<sup>1–3</sup> Among these, the ramsdellite-like  $\text{TiO}_2(\text{R})$ <sup>4</sup> and hollandite-like  $\text{TiO}_2(\text{H})$ <sup>5</sup> contain an interesting 1D channel with 3–5 Å diameter micropores. Because of the  $\text{Ti}^{4+}$  cation reducibility and porous architecture, they have been exploited as good anode materials in Li (Na)-ion batteries.<sup>6–8</sup> New  $\text{TiO}_2$  structures with stable and larger pores have been persistently pursued in experiment. To date,

porous  $\text{TiO}_2$  such as  $\text{TiO}_2$  membranes (mean pore size, around 9 Å)<sup>9,10</sup> and  $\text{TiO}_2$  xerogels (mean pore size,  $\sim 15$  Å)<sup>11</sup> have, however, either intergranular or amorphous pores, being not thermally stable above 400 °C.<sup>10,11</sup> Whether titania could have large porous crystalline phases (e.g.,  $>5$  Å) is a fundamental question.

It is known in general chemistry that tetrahedron or octahedron is a common building block for porous crystalline materials. Aluminosilicate zeolite, for example, as the most abundant microporous structures, is constituted by corner-sharing  $[\text{AlO}_4]$  or  $[\text{SiO}_4]$  tetrahedra, which can then form a variety of multiple-membered (4, 6, or 8, etc.) ring micropore structures (commonly  $<20$  Å). For  $\text{TiO}_2$ , the  $[\text{TiO}_4]$  unit is believed to be not stable. Instead, using  $[\text{TiO}_6]$  octahedron as the building block,  $\text{TiO}_2(\text{R})$  and  $-(\text{H})$  are found to be the only two known  $\text{TiO}_2$  crystals with micropores, i.e., six- and eight-member rings, respectively. By edge-sharing  $[\text{TiO}_6]$  octahedra and forming 1D  $\text{TiO}_6$  chains,  $\text{TiO}_2(\text{R})$  and  $-(\text{H})$  crystal can be considered as the assembly of 1D  $[\text{TiO}_6]$  chains via corner-sharing between chains. The presence of  $\text{TiO}_2(\text{R})$  and  $-(\text{H})$  suggests that  $\text{TiO}_2$  may have other microporous architecture with the building block other than  $[\text{TiO}_4]$  or  $[\text{TiO}_6]$ .

Recently we explore the phase space of  $\text{TiO}_2$  by utilizing a novel theoretical tool, namely, stochastic surface walking (SSW)<sup>12–17</sup> for global optimization based on density functional theory (DFT) and neural network techniques.<sup>18</sup> From more

**Received:** October 11, 2017

**Published:** November 27, 2017

than  $10^6$  minima visited by SSW global optimization, the global potential energy surface (PES) of  $\text{TiO}_2$  solid is mapped out (see the Supporting Information (SI) for calculation details and Figure S1 for the global PES). This provides the first opportunity to examine all likely  $\text{TiO}_2$  structures as guided by the total energy from quantum mechanics. Here, we report the chemistry for a new class of unprecedented microporous  $\text{TiO}_2$  crystalline phases, which feature a special  $[\text{TiO}_5]$  trigonal bipyramid building block, a large pore size (5–7 Å), and high thermal stability. We show that these microporous materials are potential anode materials for Li-ion batteries.

Figure 1 shows the energy spectrum for important crystalline phases from the global PES of  $\text{TiO}_2$ , and the crystal structures of porous  $\text{TiO}_2$  phases are highlighted (also see Figure S2). We note that different DFT functionals, i.e., PBE (Figure 1) and hybrid functional HSE06 (Figure S3), yield the similar energy spectrum for different  $\text{TiO}_2$  phases. From DFT, taking the energy of anatase as the reference (set as zero), the rutile phase is 0.09 eV/(formula unit (f.u.)) less stable than anatase and the experimentally observed  $\text{TiO}_2(\text{R})$  and  $-(\text{H})$  crystals are 0.16 eV/f.u. less stable than the common anatase phase.

From the global PES data, we identify three classes of microporous  $\text{TiO}_2$  crystals, distinguishable from the  $[\text{TiO}_x]$  building block,  $[\text{TiO}_6]$  octahedron,  $[\text{TiO}_4]$  tetrahedron, and  $[\text{TiO}_5]$  trigonal bipyramid. Obviously,  $\text{TiO}_2(\text{R})$  and  $-(\text{H})$  are the only stable microporous  $\text{TiO}_2$  crystals with the  $[\text{TiO}_6]$  octahedron building block. A  $\beta$ -cristobalite-like  $\text{TiO}_2(\beta\text{-C})$  is the most stable microporous  $\text{TiO}_2$  crystal with the  $[\text{TiO}_4]$  tetrahedron building block, but it is even less stable than  $\text{TiO}_2(\text{R})$  and  $-(\text{H})$  crystals.

Importantly, a new class of stable microporous structures constituted by the  $[\text{TiO}_5]$  trigonal bipyramid building block, namely,  $\text{TiO}_2(\text{TB})$ , are present with low energetics: the four typical  $\text{TiO}_2(\text{TB})$  crystals, as shown in Figure 1, are only 0.02–0.07 eV/f.u. less stable than the anatase phase and energetically preferable over the known (experimentally synthesized) rutile, (R), and (H) crystalline phases. They are structurally similar to the  $[\text{TiO}_3]$  building block, and other possible stable  $\text{TiO}_2(\text{TB})$  crystals can be found in Figure S4. We notice that in the known titanasilicate zeolites (JDF-L1)<sup>19</sup> similar  $[\text{TiO}_5]$  coordination has been found, which is in connection with  $[\text{SiO}_4]$  in forming the crystal. However, the crystal structure constituted by the trigonal bipyramid building block with an  $\text{AB}_2$  stoichiometry, to the best of our knowledge, has never been reported, not least because (i) five coordination is generally unfavorable in covalent bonding as predicted from hybridization orbital theory and (ii) C5 symmetry is not allowed in periodic crystals.

In Tables 1 and S1, we list the geometry parameters of typical  $\text{TiO}_2$  including four  $\text{TiO}_2(\text{TB})$  crystals. These four  $\text{TiO}_2(\text{TB})$  crystals are named as the  $\text{TiO}_2(\text{TB})\text{-I}$ ,  $\text{-II}$ ,  $\text{-III}$ , and  $\text{-IV}$ , which possess the *Imma*, *Cmcm*, *I<sub>4</sub>/mmm*, and *Imma* symmetries, respectively. They exhibit a 1D channel with large pore sizes, ranging from 5.6 to 6.7 Å. Because of the large pores, the densities of  $\text{TiO}_2(\text{TB})$  crystals decrease to 2.2–2.5 g/cm<sup>3</sup>, much smaller than other  $\text{TiO}_2$  crystals (3.3–4.1 g/cm<sup>3</sup>).

To understand the chemistry of the  $[\text{TiO}_5]$  building block, in Figure 2, we compare the architecture to form  $\text{TiO}_2(\text{TB})$  crystals by  $[\text{TiO}_5]$  trigonal bipyramid with that to form  $\text{TiO}_2(\text{R})$  and  $-(\text{H})$  crystals by  $[\text{TiO}_6]$  octahedron. By edge-sharing  $[\text{TiO}_5]$  trigonal bipyramid and forming 1D  $[\text{TiO}_5]$  nanosheets, the primary structures in Figure 2, the  $\text{TiO}_2(\text{TB})$  crystals can be considered as the assembly of 1D  $[\text{TiO}_5]$  nanosheets via corner-sharing between nanosheets. There are

Table 1. Structural Properties of  $\text{TiO}_2$  Crystal Phases<sup>a</sup>

$\text{TiO}_2$	SG	$\rho$	CN	$d_{\text{Ti-O}}$	$d_{\text{pore}}$
anatase	<i>I4<sub>1</sub>/amd</i>	3.75	6	1.97	
rutile	<i>P4<sub>2</sub>/mnm</i>	4.11	6	1.98	
(R)	<i>Pbnm</i>	3.46	6	2.04	3.64
(H)	<i>I4/m</i>	3.35	6	1.99	5.37
(TB)-I	<i>Imma</i>	2.63	5	1.92	5.77
(TB)-II	<i>Cmcm</i>	2.54	5	1.92	5.65
(TB)-III	<i>I4/mmm</i>	2.44	5	1.91	6.16
(TB)-IV	<i>Imma</i>	2.27	5	1.92	6.71
( $\beta\text{-C}$ )	<i>Fd<math>\bar{3}m</math></i>	1.79	4	1.82	5.94

<sup>a</sup>Listed data include space group (SG), density ( $\rho$ , g/cm<sup>3</sup>), coordination number (CN) of Ti, the average Ti–O bond length ( $d_{\text{Ti-O}}$ , Å), and pore size ( $d_{\text{pore}}$ , Å).

two patterns in the process of assembly, associated with the bonding types of nanosheets, i.e., monodentate (M) and bidentate (B) inside the same ring (as indicated in Figure 2), differing by the sharing pattern of the O linker atom between nanosheets. With the M and B patterns, four assembly motifs can be established that generate the typical six- and eight-member-ring microporous  $\text{TiO}_2(\text{TB})$ . These six- and eight-member rings can be considered as secondary structures, as shown in Figure 2. The six-member-ring pore is composed of two M-type and two B-type nanosheets with two assembly motifs: M-B-M-B and M-M-B-B. The eight-member-ring pore is constituted by four B-type nanosheets with the assembly motifs of B-B-B-B, or two B-type and four M-type nanosheets with the assembly motifs of B-M-M-B-M-M. The periodic  $\text{TiO}_2(\text{TB})$  crystal structures can be finally formed by further cross-linking these secondary structures.

## ■ PROPERTIES AND BONDING

The thermal stability of  $\text{TiO}_2(\text{TB})$  crystals is further examined by performing high-temperature molecular dynamics simulations based on DFT with isothermal–isobaric (NPT) ensembles. Our simulation was carried out with a large  $\text{TiO}_2(\text{TB})$  crystal supercell containing 216 atoms. The snapshots of atomic configurations of  $\text{TiO}_2(\text{TB})$  crystals during MD simulations are shown in Figures 3a and S5. After heating at 1073 K for 4.5 ps with a time step of 1.5 fs, no obvious structure reconstruction or phase transition is found in these  $\text{TiO}_2(\text{TB})$  crystals, which indicates that the  $\text{TiO}_2(\text{TB})$  crystals are kinetically stable and the transition from them to other crystal phases is separated by high barriers. In addition, the calculated phonon dispersion spectrum also confirms their structural stabilities (Figure S6): no imaginary modes are present in the entire Brillouin zone.

Next, we computed the mechanical property of  $\text{TiO}_2(\text{TB})$  as measured by the bulk moduli using the Voigt–Reuss–Hill (VRH) approximation (Table S1). We found that the bulk modulus of  $\text{TiO}_2(\text{TB})$  crystals ( $\sim 100$  GPa) is comparable with those of (R) and (H) crystals ( $\sim 110$  GPa) and their values are generally lower than those of denser anatase and rutile phases ( $>180$  GPa). This is reasonable since the denser phase is expected to be less compressible.

Considering the interesting porous network structure, high thermal stability, and good mechanic stability, it is important to ask what is the origin for the stability of these  $\text{TiO}_2(\text{TB})$  crystals with the unusual  $[\text{TiO}_5]$  trigonal bipyramid building block. Such penta-coordination is believed to be unfavorable

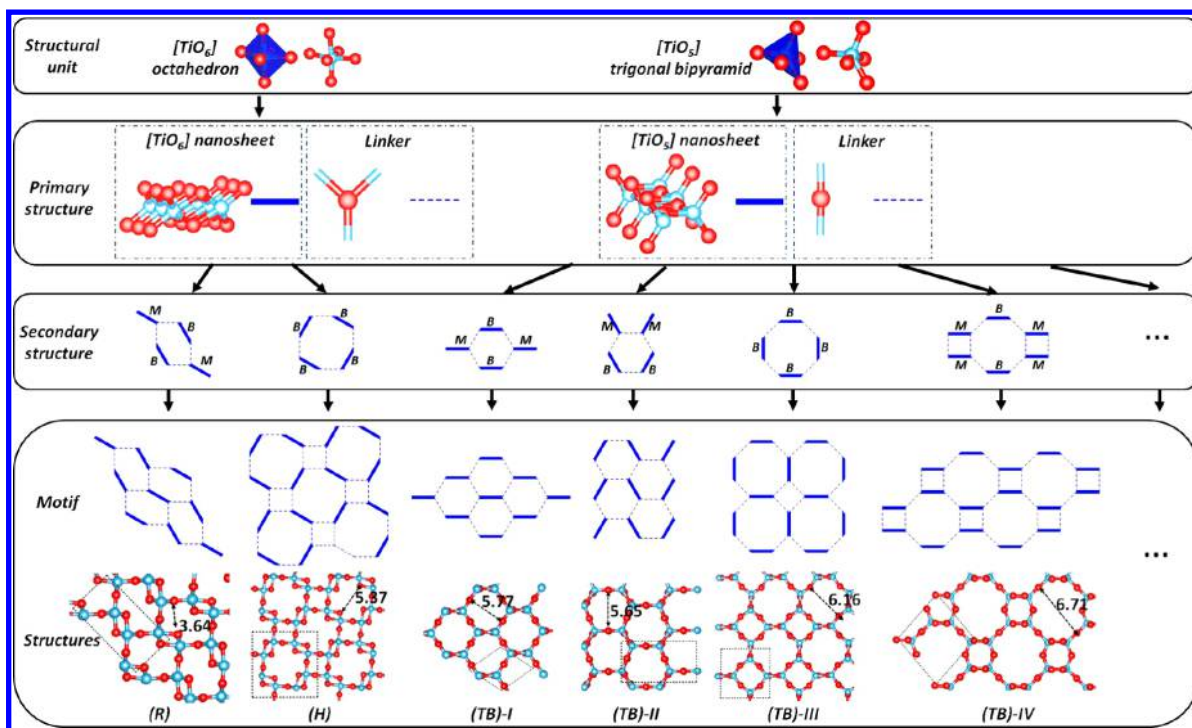


**Figure 2.** Building architecture for porous TiO<sub>2</sub> crystals. All porous TiO<sub>2</sub> crystals show 1D channel micropores but differ in the building block, where TiO<sub>2</sub>(R) and -(H) have a common [TiO<sub>6</sub>] octahedron unit while TiO<sub>2</sub>(TB) features a [TiO<sub>5</sub>] trigonal bipyramid structure unit.

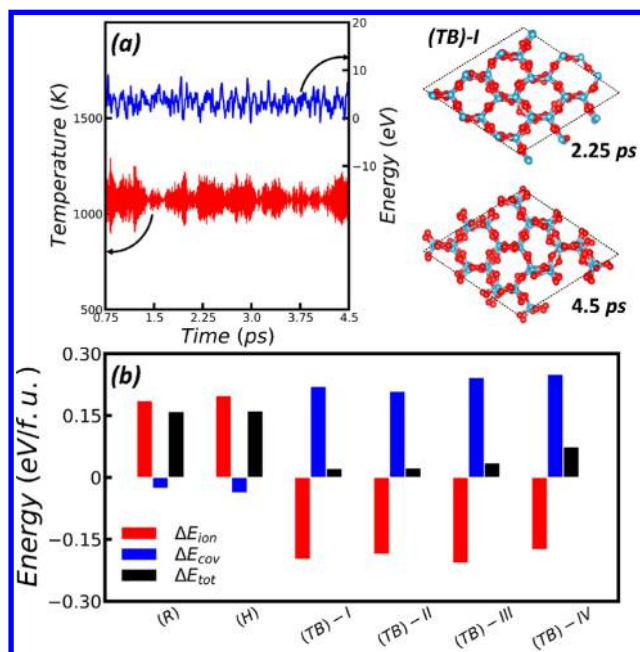


**Figure 3.** (a) First-principles MD simulation of TiO<sub>2</sub>(TB)-I crystal at 1073 K together with the snapshots at 2.25 and 4.5 ps. (b) Energy decomposition of TiO<sub>2</sub> porous crystals using  $E_{\text{tot}} = E_{\text{cov}} + E_{\text{ion}}$  where  $E_{\text{cov}}$  and  $E_{\text{ion}}$  represent the covalent and ionic bonding contributions in DFT total energy  $E_{\text{tot}}$ , respectively. All three terms ( $\Delta E$ ) are then referenced to those of TiO<sub>2</sub> anatase phase.

due to the splitting symmetry of five d-orbitals that prefers either octahedron ( $t_{2g}-e_g$ ) or tetrahedron ( $t_2-e$ ).

To understand this, we have performed the following analysis on the energetics of the ionic crystals. The total energy is divided into two parts:  $E_{\text{tot}} = E_{\text{cov}} + E_{\text{ion}}$ , where  $E_{\text{cov}}$  represents the covalence bonding energy from orbital mixing and  $E_{\text{ion}}$

represents the ionic bonding energy due to the electrostatic interaction of ions. By computing  $E_{\text{tot}}$  from DFT and  $E_{\text{ion}}$  from Ewald electrostatics using the Hirshfeld net atomic populations,<sup>20</sup> we can then deduce the contribution of covalent bonding. To compare their relative magnitude, we calculate the difference of the three energy terms for different crystals with respect to those of the anatase phase, i.e.,  $\Delta E_{\text{tot}}$ ,  $\Delta E_{\text{cov}}$ , and  $\Delta E_{\text{ion}}$  (Figure 3b). We found that  $\Delta E_{\text{ion}}$  for TiO<sub>2</sub>(R) and -(H) crystals are 0.19 eV/f.u., indicating their ionic bonding is weaker than that of anatase. By contrast,  $\Delta E_{\text{ion}}$  for TiO<sub>2</sub>(TB) crystals is -0.19 eV/f.u., showing much stronger ionic bonding than anatase. Considering the similar Hirshfeld net atomic populations for all these crystals (Table S2), it is possible to attribute the difference in the ionic bonding interaction to the geometry in different crystals. Obviously, the Ti–O distance in TiO<sub>2</sub>(TB) crystals (~1.92 Å) is shorter compared to other crystals (~2.01 Å for TiO<sub>2</sub>(R) and -(H) and 1.97 Å for anatase, Table 1) and the O–O repulsion is lower in the five-coordination unit. For the covalent bonding, there is little difference between TiO<sub>2</sub>(R) and -(H) and anatase, apparently because of their same coordination environment ([TiO<sub>6</sub>] octahedron building block). For TiO<sub>2</sub>(TB), the [TiO<sub>5</sub>] trigonal bipyramid building block indeed has a weak covalent interaction ( $\Delta E_{\text{cov}} = 0.22$  eV/f.u.). Therefore, we can conclude that the stronger ionic interaction in TiO<sub>2</sub>(TB) crystals is key for their high stability, which compensates for the weaker covalent bonding.

## APPLICATIONS IN LI-ION BATTERY

Finally, we have examined the potential applications for TiO<sub>2</sub>(TB) materials. Obviously, the large 1D tunnel of TiO<sub>2</sub>(TB) can be a potential mass transport channel for ion diffusion and insertion, which are key components as anode material in Li-ion battery. In this work, we examined the structure change and the average voltage of Li<sub>x</sub>TiO<sub>2</sub> for Li

insertion of  $\text{TiO}_2(\text{TB})$ , as shown in Figures 4 and S7. The structure change is critical to the performance of the anode

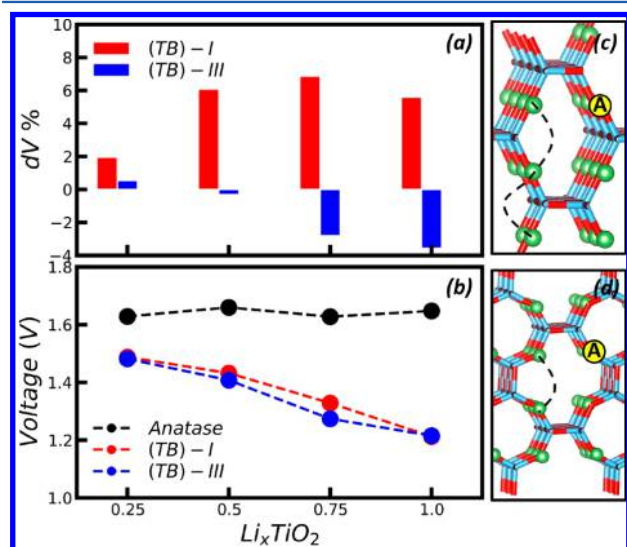


**Figure 4.** Performance of  $\text{TiO}_2(\text{TB})$ -I and -III as Li-ion battery anode at different Li fraction  $x$  ( $\text{Li}_x\text{TiO}_2$ ). (a) Plot for volume change  $dV\%$  against Li fraction; (b) plot for the average voltage  $V_0$  against Li fraction; (c, d) structures of  $\text{Li}_x\text{TiO}_2(\text{TB})$ -I and -III at  $x = 1$ . Li atom, green ball.

materials, which can usually be measured by the volume expansion percentage  $dV\%$ , given by  $dV\% = \left[ \frac{V - V_{\text{ref}}}{V_{\text{ref}}} \right] \times 100$ .<sup>21</sup>

For the average voltage, it can be calculated as follows. The formation energy  $\Delta E_f$  is first calculated using the equation  $\Delta E_f = E_{\text{Li}_x\text{TiO}_2} - nE_{\text{Li}} - E_{\text{TiO}_2}$ , which reflects the thermodynamics of lithiation with reference to the bulk Li metal and bulk  $\text{TiO}_2(\text{TB})$  crystal. Using  $\Delta E_f$ , the average voltage  $V_0$  can then be calculated via the Nernst equation,  $V_0 = -\Delta E_f/nF$  ( $F$ , Faraday constant).<sup>22</sup> For a good anode material, the  $V_0$  should be positive but close to zero in order to yield the high output voltage.

By computing the  $\text{Li}_x\text{TiO}_2(\text{TB})$  structures, we found that, during the lithiation process, Li ions will diffuse into the channel and anchor to the center of two bridge O anions (labeled as A sites in Figure 4c,d), while leaving the channel space open. The diffusion of Li ions between neighboring A sites is facile along the dashed lines in Figure 4c,d with a barrier of  $\sim 0.4$  eV (Figure S8). Importantly, these  $\text{TiO}_2(\text{TB})$  crystals after Li insertion exhibit a low volume expansion ( $<7\%$ ) even at the  $\text{Li}:\text{TiO}_2 = 1:1$  ratio. The  $\text{TiO}_2(\text{TB})$ -III crystal, for its large channel, even has a slight volume reduction by 3.5% at the  $\text{Li}:\text{TiO}_2 = 1:1$  ratio. These values in volume change are comparable with that for anatase (3.2%,  $\text{Li}_{0.5}\text{TiO}_2$ ) and  $\text{TiO}_2(\text{R})$  crystal (4.2%,  $\text{Li}_{0.5}\text{TiO}_2$ ) after Li insertion,<sup>21,23,24</sup> but considerably smaller compared to that in commercial graphite ( $\sim 300\%$ ). This offers the possibility of  $\text{TiO}_2(\text{TB})$  as a fast-charging anode material. As for the average voltage, while those for anatase and  $\text{TiO}_2(\text{R})$  crystals are around 1.6 V,  $\text{TiO}_2(\text{TB})$  crystals have a smaller  $V_0$ , 1.51 to 1.22 V, depending on the Li fraction (Figure 4b). The smaller  $V_0$  indicates that  $\text{TiO}_2(\text{TB})$  crystals can have a higher output voltage compared to other  $\text{TiO}_2$  phases. Based on the data on volume change, diffusion barrier, and average voltage, we predict that  $\text{TiO}_2(\text{TB})$  crystals are good anode materials for Li-ion battery.

To recap, guided by global potential energy surface data of  $\text{TiO}_2$ , we predict a class of new microporous  $\text{TiO}_2$  crystals  $\text{TiO}_2(\text{TB})$  with an unusual  $[\text{TiO}_5]$  trigonal bipyramid building block, which are stable from thermodynamics and kinetics aspects. They are also promising for fast-charging anode material for Li-ion battery. These findings may motivate further experimental efforts for synthesizing and utilizing microporous  $\text{TiO}_2$  crystalline materials.

## ■ ASSOCIATED CONTENT

### Supporting Information

The Supporting Information is available free of charge on the ACS Publications website at DOI: 10.1021/acsam.7b00021.

Additional details on calculation methods; potential energy surface of  $\text{TiO}_2$ ; lattice parameters for crystalline phases; phonon spectrum; energy spectrum of HSE06; AIMD results; atomic XYZ positions for  $\text{TiO}_2(\text{TB})$  crystals (PDF)

## ■ AUTHOR INFORMATION

### Corresponding Author

\*E-mail: zpliu@fudan.edu.cn.

### ORCID

Zhi-Pan Liu: 0000-0002-2906-5217

### Notes

The authors declare no competing financial interest.

## ■ ACKNOWLEDGMENTS

This work was supported by the National Science Foundation of China (Grant No. 21533001, 21573149), the 973 program (Grant No. 2013CB834603), and the Science and Technology Commission of Shanghai Municipality (Grant No. 08DZ2270500).

## ■ REFERENCES

- Zhang, H.; Banfield, J. F. Structural characteristics and mechanical and thermodynamic properties of nanocrystalline  $\text{TiO}_2$ . *Chem. Rev.* **2014**, *114*, 9613–9644.
- Wang, L.; Sasaki, T. Titanium oxide nanosheets: graphene analogues with versatile functionalities. *Chem. Rev.* **2014**, *114*, 9455–9486.
- Sasaki, T.; Watanabe, M.; Hashizume, H.; Yamada, H.; Nakazawa, H. Macromolecule-like aspects for a colloidal suspension of an exfoliated titanate. Pairwise association of nanosheets and dynamic reassembling process initiated from it. *J. Am. Chem. Soc.* **1996**, *118*, 8329–8335.
- Akimoto, J.; Gotoh, Y.; Oosawa, Y.; Nonose, N.; Kumagai, T.; Aoki, K.; Takei, H. Topotactic oxidation of ramsdellite-type  $\text{Li}_{0.5}\text{TiO}_2$ , a new polymorph of titanium dioxide:  $\text{TiO}_2(\text{R})$ . *J. Solid State Chem.* **1994**, *113*, 27–36.
- Latroche, M.; Brohan, L.; Marchand, R.; Tournoux, M. New hollandite oxides:  $\text{TiO}_2(\text{H})$  and  $\text{K}_{0.06}\text{TiO}_2$ . *J. Solid State Chem.* **1989**, *81*, 78–82.
- Sakao, M.; Kijima, N.; Akimoto, J.; Okutani, T. Synthesis, crystal structure, and electrochemical properties of hollandite-type  $\text{K}_{0.008}\text{TiO}_2$ . *Solid State Ionics* **2012**, *225*, 502–505.
- Perez-Flores, J.; Baetz, C.; Kuhn, A.; Garcia-Alvarado, F. Hollandite-type  $\text{TiO}_2$ : a new negative electrode material for sodium-ion batteries. *J. Mater. Chem. A* **2014**, *2*, 1825–1833.
- Zhu, G.-N.; Wang, Y.-G.; Xia, Y.-Y. Ti-based compounds as anode materials for Li-ion batteries. *Energy Environ. Sci.* **2012**, *5*, 6652–6667.
- Puhlfürb, P.; Voigt, A.; Weber, R.; Morbé, M. Microporous  $\text{TiO}_2$  membranes with a cut off  $< 500$  Da. *J. Membr. Sci.* **2000**, *174*, 123–133.

- (10) Sekulić, J.; ten Elshof, J. E.; Blank, D. H. A. A microporous titania membrane for nanofiltration and pervaporation. *Adv. Mater.* **2004**, *16*, 1546–1550.
- (11) Xu, Q.; Anderson, M. A. Sol–gel route to synthesis of microporous ceramic membranes: preparation and characterization of microporous TiO<sub>2</sub> and ZrO<sub>2</sub> xerogels. *J. Am. Ceram. Soc.* **1994**, *77*, 1939–1945.
- (12) Shang, C.; Liu, Z.-P. Stochastic surface walking method for structure prediction and pathway searching. *J. Chem. Theory Comput.* **2013**, *9*, 1838–1845.
- (13) Zhang, X.-J.; Shang, C.; Liu, Z.-P. From atoms to fullerene: stochastic surface walking solution for automated structure prediction of complex material. *J. Chem. Theory Comput.* **2013**, *9*, 3252–3260.
- (14) Shang, C.; Zhang, X.-J.; Liu, Z.-P. Stochastic surface walking method for crystal structure and phase transition pathway prediction. *Phys. Chem. Chem. Phys.* **2014**, *16*, 17845–17856.
- (15) Guan, S.-H.; Zhang, X.-J.; Liu, Z.-P. Energy landscape of zirconia phase transitions. *J. Am. Chem. Soc.* **2015**, *137*, 8010–8013.
- (16) Zhu, S.-C.; Xie, S.-H.; Liu, Z.-P. Nature of rutile nuclei in anatase-to-rutile phase transition. *J. Am. Chem. Soc.* **2015**, *137*, 11532–11539.
- (17) Li, Y.-F.; Zhu, S.-C.; Liu, Z.-P. Reaction Network of Layer-to-Tunnel Transition of MnO<sub>2</sub>. *J. Am. Chem. Soc.* **2016**, *138*, 5371–5379.
- (18) Huang, S.-D.; Shang, C.; Zhang, X.-J.; Liu, Z.-P. Material discovery by combining stochastic surface walking global optimization with a neural network. *Chem. Sci.* **2017**, *8*, 6327–6337.
- (19) Roberts, M.; Sankar, G.; Thomas, J.; Jones, R.; Du, H.; Chen, J.; Pang, W.; Xu, R. Synthesis and structure of a layered titanosilicate catalyst with five-coordinate titanium. *Nature* **1996**, *381*, 401–404.
- (20) Hirshfeld, F. L. Bonded-atom fragments for describing molecular charge densities. *Theor. Chim. Acta.* **1977**, *44*, 129–138.
- (21) Kerisit, S.; Rosso, K. M.; Yang, Z.; Liu, J. Computer simulation of the phase stabilities of lithiated TiO<sub>2</sub> polymorphs. *J. Phys. Chem. C* **2010**, *114*, 19096–19107.
- (22) Aydinol, M.; Kohan, A.; Ceder, G.; Cho, K.; Joannopoulos, J. Ab initio study of lithium intercalation in metal oxides and metal dichalcogenides. *Phys. Rev. B: Condens. Matter Mater. Phys.* **1997**, *56*, 1354.
- (23) Kuhn, A.; Baehtz, C.; Garcia-Alvarado, F. Structural evolution of ramsdellite-type Li<sub>x</sub>Ti<sub>2</sub>O<sub>4</sub> upon electrochemical lithium insertion–deinsertion (0 ≤ x ≤ 2). *J. Power Sources* **2007**, *174*, 421–427.
- (24) Cava, R.; Murphy, D.; Zahurak, S.; Santoro, A.; Roth, R. The crystal structures of the lithium-inserted metal oxides Li<sub>0.5</sub>TiO<sub>2</sub> anatase, LiTi<sub>2</sub>O<sub>4</sub> spinel, and Li<sub>2</sub>Ti<sub>2</sub>O<sub>4</sub>. *J. Solid State Chem.* **1984**, *53*, 64–75.